Modification of a natural zeolite with Fe(III) for simultaneous phosphate and ammonium removal from aqueous solutions

Diana Guaya [a, b*], Cesar Valderrama [a], Adriana Farran [a], José Luis Cortina [a, c]

[a] Department of Chemical Engineering, Universitat Politècnica de Catalunya-Barcelona Tech (UPC), Barcelona, Spain

[b] Departament of Chemistry, Universidad Técnica Particular de Loja, Loja, Ecuador

[c] Water Technology Center CETaqua, Barcelona, Spain

*Correspondence should be addressed to: Diana Guaya

Email: deguaya@utpl.edu.ec

Abstract

The incorporation of Fe(III) was performed in a natural clinoptilolite (Z-N) for simultaneous phosphate and ammonium removal. The existence of hydroxyl groups (≅Fe-OH) in the iron zeolite (Z-Fe) enhances the phosphate uptake from 0.6±0.1 mg-P/g in Z-N to 3.4±0.2 mg-P/g in Z-Fe. However, the ammonium sorption capacity slightly decreases from 33±2 mg-N/g in Z-N to 27±2 mg-N/g in Z-Fe. The equilibrium and kinetics sorption were well explained by the Langmuir isotherm and the intraparticle diffusion model, respectively. Both the phosphate and ammonium uptake were slightly affected by the coexistence of competing ions. The phosphate sorption capacity of iron zeolite was decreased in the regeneration cycles. The desorption using a 1 M NaOH solution under dynamic conditions provided higher enrichment factors for ammonium than phosphate.

Keywords: clinoptilolite; iron; phosphate; ammonium; sorption; kinetic

1. Introduction

Eutrophication, is a serious environmental problem associated with phosphate and ammonium overloading in surface waters due to municipal effluents and agricultural runoff [1]. Therefore, the implementation of wastewater purification technologies for both phosphate and ammonium removal is required [2, 3]. Natural and synthetic zeolites are crystalline microporous aluminosilicates that are widely used in separation and purification processes and a promising material for environmental applications [4] due to their high abundance, availability and low cost [5-7]. In addition, zeolites can be used as substrates for supporting and impregnating metallic hydroxides for oxyanion uptake applications (i.e., arsenic and phosphate) [8, 9]. Surface-modified adsorbents have become more prominent in recent years. In addition to granular media, such as granular ferric hydroxides (GFH) and granular activated carbon (GAC) that are used for anions adsorption, other iron composites have been used to confine iron oxide particles in the pores of the support. A convenient method to control aggregation and particle size involves the preparation of iron hydroxide particles (e.g., akaganeite) in a template, such as clay [10, 11], polymer [12, 13] or Fe-exchanged natural zeolite [14].

The modification of zeolites with Fe(III) is typically performed in two stages as follows: i) the conversion of the zeolite to the Na^+ form using NaCl, NaOH and NaOH/NaCl solutions and ii) the conversion of the sodium form of the zeolite (Z^-Na^+) to the Fe(III) form using typical $FeCl_3$ solutions. When the modification process is carried out under acidic conditions, Na^+ ions are exchanged by Fe(III) cationic species and, to a lesser extent, the formation of hydrated iron oxides [15, 16]. Under basic conditions, the formation of hydrated iron hydroxide particles is the main modification mechanism [17, 18]. In general, the mineral properties of the zeolite support are not modified. However, a slight increase in the surface area has been associated with the formation of hydrated mineral oxides occupying both the surface and channels of the porous structure of zeolitic material [19]. The application of Fe(III) modified zeolites as well as Al(III), Mn(II) or Zr(IV) for

the removal of oxyanionic species has been primarily focused on the removal of toxic elements, such as As(III)/As(V) [18], and other anions, such as fluoride [20]. Most of these studies of modified zeolites have focused on the removal mechanism with little attention to their possible regeneration.

This study describes the modification of a natural zeolite (clinoptilolite) with Fe(III) to promote the formation of >FeOH surface groups on the zeolites structure to favour the simultaneous uptake of cationic (ammonium) and anionic ($H_2PO_4^-$/HPO_4^{2-}) species; to evaluate the sorption performance and the potential regeneration and re-use of the Z-Fe zeolite via sorption and desorption cycles for tertiary wastewater treatment applications. The objectives of this work are as follows: (i) to incorporate Fe(III) into natural zeolite, (ii) to characterize the modified zeolite, (iii) to study the influence of pH and concentration on the phosphate and ammonium sorption onto the modified zeolite, (iv) to determine the equilibrium and kinetic sorption parameters, (v) to determine the sorption selectivity of common ions in wastewater effluents and (vi) to evaluate its performance in sorption and desorption cycles via dynamic experiments.

2. Materials and methods

2.1. Incorporation of Fe(III) to the natural zeolite

A natural zeolite (Z-N) obtained from the Zeocem Company (Slovak Republic) was washed and dried at 80 °C for 24 hours. The experiments were performed in batch (particles < 200 μm) and fixed-bed (< 800 μm) configurations. Z-N was modified to the iron form using an adaptation of the method reported by Jiménez – Cedillo et al. [21]. The Z-N sample (30 g) was treated in 250 mL of NaCl (0.1 M) two consecutive times under reflux for 4 h to obtain the sodium form of the zeolite (Z-Na). Then, the Z-Na sample (30 g) was treated two consecutive times by refluxing in 250 mL of $FeCl_3$ (0.1 M) for 4 h to obtain the iron zeolite (Z-Fe). After treatment, the samples were washed until no chloride was detected using an $AgNO_3$ test followed by drying at 80 °C for 24 hours.

2.2. Physicochemical characterization of the zeolites

A powder X-ray diffractometer (D8 Advance A25 Bruker) was used for X-ray diffraction (XRD) characterization of the Z-N, Z-Na and Z-Fe samples. The chemical composition and morphology of the samples were determined using a field emission scanning electron microscope (JEOL JSM-7001F) coupled to an energy dispersive spectroscopy system (Oxford Instruments X-Max). The infrared absorption spectra were recorded on a Fourier transform FTIR 4100 (Jasco) spectrometer in a range of 4000 to 550 cm^{-1}. The nitrogen gas adsorption method was used to determine the specific surface area of the Z-N, Z-Na and Z-Fe samples on an automatic sorption analyser (Micrometrics). The tests were replicated at least four times for each sample, and the average values are reported.

2.3. Equilibrium and kinetic batch sorption studies

The batch equilibrium sorption experiments were carried out using a standard methodology that has been previously reported [22]. Weighed amounts of the dry samples (particle size < 200 µm) were shaken overnight in 25 mL of a solution containing various phosphate (P) and ammonium (N) concentrations. The following types of experiments were performed:

i) Sorption capacity as a function of phosphate and ammonium concentration: The Z-N and Z-Fe samples (0.25 g) were equilibrated in solutions without pH adjustment using concentrations ranging 1 to 2000 mg-P/L and 10 – 5000 mg-N/L.

ii) Sorption capacity as a function of equilibrium pH: The Z-Fe (0.1 g) sample was added to 25 mg-P/L and 25 mg-N/L solutions (pH adjusted from 2 to 11).

iii) Sorption capacity as a function of phosphate and ammonium concentration in the presence of individual ions and mixtures of common competing ions present in wastewater effluents: By addition of the Z-Fe sample (0.1 g) to solutions (without pH adjustment) containing 25 mg-P/L, 25 mg-N/L and 25 mg/L of the competing ion. The ion concentrations were fixed at the average annual composition of the stream from a tertiary treatment including a reverse osmosis step at

the El Prat wastewater treatment plant (Barcelona – Spain). The solution consisted of: chloride (625 mg/L), bicarbonate (325 mg/L), sulfate (200 mg/L), nitrate (30 mg/L), sodium (260 mg/L), calcium (160 mg/L), magnesium (50 mg/L) and potassium (40 mg/L). Finally, the Z-Fe sample (0.25 g) was equilibrated in a solution containing concentrations ranging from 1 to 2000 mg-P/L and 10 – 5000 mg-N/L with the mixed ion solutions.

iv) Batch kinetic sorption experiments: The Z-Fe (0.1 g) sample was equilibrated in a solution containing 20 mg-N/L and 10 mg-P/L. The tubes were withdrawn sequentially at specific time intervals. All of the tests were performed at 200 rpm and room temperature (21±1 °C) in triplicate, and the average values are reported. The samples were centrifuged for 10 min and filtered (45 µm) prior to analysis. The concentrations of the phosphate and ammonium ions were determined in the initial and remaining aqueous solution. In addition, the loaded zeolite samples were examined by field scanning electron microscopy, and the mineral phases were identified by X-Ray diffraction.

2.4. Phosphate speciation in the loaded Z-Fe samples by fractionation assays.

The fractionation of phosphorus immobilized in loaded Z-Fe was performed based on a modified three sequential step extraction protocol [23]. The Z-Fe sample (0.25 g) was equilibrated in 25 mL of a 25 mg-P/L solution. The loaded sample was washed and dried prior to the extraction trials. The loosely bound phosphorus fraction (LB-P) was determined by two consecutive extractions of the Z-Fe loaded sample (0.25 g) in 20 mL of 1 M NH_4Cl (pH 7). The iron and aluminum fraction ($Fe^{+}Al$)-P was determined by two consecutive extractions in 20 mL of 0.1 M NaOH followed by extraction in 1 M NaCl. Finally, the phosphorus linked to the calcium and magnesium compounds ($Ca^{+}Mg$)-P was determined by two consecutive extractions in 20 mL of 0.5 M HCl. The residual phosphorus (R-P) was calculated based on the mass balance between the phosphorus adsorbed and the extracted fractions. The tests were performed at 200 rpm in triplicate at 21±1 °C, and the average data are reported.

2.5. Phosphate and ammonium batch desorption studies

The Z-Fe sample (0.5 g < 200 μm) was added to 25 mL of a solution containing 25 mg-P/L and 25 mg-N/L. The loaded sample was washed and dried followed by equilibration in 25 mL of the elution solution: (i.e., NaOH (1 M), $NaHCO_3$ (0.1 M), Na_2CO_3 (0.1 M) and $NaHCO_3$/Na_2CO_3 (0.1 M)). The tests were performed in two sorption – desorption cycles at 200 rpm in triplicate at 21±1 °C, and average values are reported.

2.6. Phosphate and ammonium sorption and desorption column studies

The Z-Fe samples (<800 μm) were packed in a glass column (15 mm x 100 mm). The expected values of the effluent streams from secondary treatment at the El Prat wastewater treatment plant (Barcelona – Spain) were considered for the feed composition (i.e., phosphate (12.5 mg/L), ammonium (25 mg/L), chloride (312.5 mg/L), bicarbonate (162.5 mg/L), sulfate (10 mg/L), nitrate (15 mg/L), sodium (130 mg/L), calcium (80 mg/L), magnesium (25 mg/L) and potassium (20 mg/L)). The sorption under dynamic conditions was evaluated in the presence and absence of competing ions with a countercurrent flow rate of 1.85 mL/min. Then, Z-Fe was saturated in the absence of competing ions and regenerated using a 1 M NaOH solution at a flow rate of 0.5 mL/min.

2.7. Analytical methods

Standard methods were used for phosphate (P) and ammonium (N) determination [24]. The vanadomolybdophosphoric acid colorimetric method (4500-P C) allowed for P quantification, and the ammonia-selective electrode method (4500-NH3 D) was employed for N determination. The ions were determined using a Thermo Scientific Ionic Chromatograph (Dionex ICS-1100 and ICS-1000).

3. Results and discussion

3.1. Characterization of modified Fe(III) zeolite

The XRD patterns of Z-N, Z-Na and Z-Fe (supporting information Figure S1) indicated that clinoptilolite as the main crystalline phase, which coexisted with quartz and albite. The Z-Na sample was an intermediate stage in the zeolite modification to the iron form due to the easy sodium removal in ion exchange applications [25]. The existence of akaganeite (β-FeOOH) as the crystalline iron phase was observed in Z-Fe, which is in contrast to the reports of amorphous iron oxide species forming on natural zeolite surfaces [8, 21, 26]. The Z-Na and Z-Fe spectra exhibited the zeolite characteristic reflections (i.e., 2θ at 9.92°, 11.23°, 17.36°, 22.52° and 32.08°), which did not change. The small changes in the intensity of the reflections observed in the Z-Fe spectra resulted from the occupation of cation exchange sites by iron ions due to the $FeCl_3$ treatment. In addition, the specific surface area (19.8±0.3 m^2/g) of Z-N and Z-Fe was the same.

The FSEM-EDX analysis indicated that the chemical composition of clinoptilolite consisted of O, Na, Mg, Al, Si, K, Ca, Ti and Fe as the main elements (Table 1).

In the Z-Na sample, the increase in the Na^+ content was due to the cationic exchange reaction between the Mg^{2+}, K^+ and Ca^{2+} ions. The iron content in Z-Fe exhibited an eight-fold increase due to ion exchange between K^+, Mg^{2+}, and Ca^{2+}. In addition, it is important to note the existence of chloride (1.1%) in the modified zeolite, which is consistent with previously reported results for natural or synthetic zeolites [15, 22]. Unfortunately, no discussion has been provided in these previous studies. The presence of chloride in the sample is associated with the presence of Fe-Cl complexes (e.g., $FeCl^{2+}$ and $FeCl_2^+$), which are the predominant species in the $FeCl_3$ solutions used to modify the zeolites. The species distribution diagram for the $FeCl_3$ solution is provided in Figure S2 in the supporting information. The modification process of the zeolite can be described by exchange reactions involving Fe-Cl complexes (Eq. (1-3)) even though it could not be discarded the exchange with Fe^{+3} ions.

$$>ZO^-Na^+ + FeCl_2^+ \leftrightarrow >ZO^- FeCl_2^+ + Na^+ \quad (1)$$

$$2(>ZO^-Na^+) + FeCl^{+2} \leftrightarrow (>ZO^-)_2(FeCl^{+2}) + 2\ Na^+ \quad (2)$$

$$3(>ZO^-Na^+) + Fe^{+3} \leftrightarrow (>ZO^-)_3Fe^{+3} + 3\,Na^+ \quad (3)$$

where $>ZO^-$ represents the zeolitic structure.

A network of crystal clusters with a homogeneous size distribution was identified in the FSEM image of the Z-N sample (supporting information Figure S3a). The crystals of clinoptilolite displayed the characteristic plate-like morphology with large cavities and entries in to the channels inside the zeolite framework [27]. Notably, some lamellar crystals and small particles covered the surface of Z-Na and Z-Fe (supporting information Figures S3b, c), confirming that sodium and iron modification was achieved in clinoptilolite.

The FTIR spectra of Z-N, Z-Na and Z-Fe (supporting information Figure S4) displayed peaks between 798 cm^{-1} and 547 cm^{-1} that correspond to the stretching bridges of the Al-O-Si and Si-O-Si groups. The stretching vibration of the Si–O groups corresponds to the band at ~1100 cm^{-1}, and the deformation vibration of water was located at ~1630 cm^{-1}. The hydroxyl groups of the zeolitic structure are associated with the peaks in the range from 3700 cm^{-1} to 3100 cm^{-1} [4, 28]. The Z-N (Figure S4a) and Z-Na (Figure S4b) spectra exhibited minimal differences, which is typical for ion exchange between cations with a similar valence [29]. The Z-Fe spectra exhibit some changes in comparison to Z-N due to the ion exchange with the trivalent Fe(III) (Figure S4c). The new bands located at 1396 cm^{-1}, 1455 cm^{-1} and 1541 cm^{-1} as well as the shift at 3396 cm^{-1} are related to the presence of the surface iron hydroxide groups (≅FeOH) [30, 31]. The formation of (≅FeOH) is caused by the modification step due to the strong acidity of the Fe(III) species even at low pH values (supporting information Figure S2), promoting the formation of $Fe(OH)_2^+$ and $Fe(OH)^{2+}$ (e.g., $(>ZO^-)_2(FeOH^{2+})$ or $>ZO^-FeOH_2^+$). In addition, a fraction of Fe(III) will be in the ≅ Fe-OH form (e.g., $(Fe(OH)_3(s))$).

3.2. Phosphate and ammonium equilibrium isotherms

The equilibrium uptake for phosphate and ammonium (q_e) was calculated using Eq. 4.

$$q_e = (C_o - C_e) \times \frac{v}{w} \quad (4)$$

where C_o (mg/L) and C_e (mg/L) represent the initial and equilibrium concentrations, respectively, v (L) is the aqueous solution volume and w (g) is the mass of the zeolite. The phosphate and ammonium equilibrium sorption was evaluated according to the Langmuir (Eq. 5) and Freundlich (Eq. 6) isotherms:

$$\frac{C_e}{q_e} = \frac{1}{K_L . q_m} + \frac{C_e}{q_m} \quad (5)$$

$$\log q_e = \log K_F + \frac{1}{n} log\ C_e \quad (6)$$

where q_m (mg/g) is the maximum sorption capacity, K_L (L/mg) is the Langmuir sorption equilibrium constant and K_F ((mg/g)/(mg/L)$^{1/n}$) is the Freundlich equilibrium sorption constant.

The Langmuir isotherm provided a better description of the phosphate and ammonium equilibrium sorption ($R^2 \geq 0.99$) compared with the Freundlich isotherm (Table 2 and Figure 1), which only describes the experimental data at low concentrations levels. These results suggest that the availability of specific and equal affinity sites on the zeolite for monolayer and homogenous sorption or/and ion exchange. The phosphate maximum sorption capacity exhibited a six-fold increase in Z-Fe (3.4±0.2 mg-P/g) compared with Z-N (0.6±0.1 mg-P/g). In contrast, a decrease in ammonium capacity from 33±2 mg-N/g in Z-N to 27±2 mg-N/g in Z-Fe was observed.

The phosphate removal was not dependent on the pH in the range of 2 to 11 (Figure 2). The sorption mechanism of the phosphate oxyanion (H_2PO^{4-} - HPO_4^{2-} - PO_4^{3-}) is associated with the formation of monodentate and bidentate complexes with the hydroxyl surface groups of both of the exchanged iron complexes on the cation exchange positions or on the hydrated iron oxides (≅FeOH groups) inside the zeolite micropores (specific adsorption), which is represented by Eq. 7 [32-34]; or by means of columbic forces depending of the pH_{pzc} (non-specific adsorption), as shown in Eqs. 8 and 9 [35].

$$\mathrm{H_2PO_4^-} \quad \mathrm{Z-Fe-O-\overset{\overset{OH}{|}}{\underset{\underset{O}{\|}}{P}}-OH} \quad + OH^- \quad Monodentate$$

$$Z-Fe-OH + \xrightarrow[pH \geq pH_{PZC}]{Complexation} \begin{matrix} \mathrm{Z-Fe} < \begin{matrix} O \\ O \end{matrix} > P \leqslant \begin{matrix} OH \\ O \end{matrix} & + OH^- & Bidentate\ Mononuclear \\ \mathrm{Z-Fe-O} \\ \mathrm{Z-Fe-O} \end{matrix} > P \leqslant \begin{matrix} OH \\ O \end{matrix} \quad + 2OH^- \quad Bidentate\ Binuclear \quad (7)$$

$\mathrm{HPO_4^{2-}}$

$$Z-Fe-OH \xrightarrow[pH < pH_{PZC}]{Protonation} Z-Fe-OH^{2+} \xrightarrow[\mathrm{H_2PO_4^-/HPO_4^{2-}}]{Electrostatic\ attraction} \begin{matrix} Z-Fe-OH^{2+} \ldots \mathrm{H_2PO_4^-} \\ Z-Fe-OH^{2+} \ldots \mathrm{HPO_4^{2-}} \end{matrix} \quad (8)$$

$$Z-Fe-OH \xrightarrow[pH \gg pH_{PZC}]{Hydroxilation} Z-Fe-O^- + H_2O \quad (9)$$

The reduction of the P sorption capacity above a pH of 8, indicates the acid-base properties of the hydrated iron oxides formed during the impregnation processes with a pH_{PCZ} close to 8. This behaviour is in agreement with published data for the akaganeite minerals [36] and ion-exchange resins impregnated with hydrated iron oxides [37, 38].

The electrostatic interactions of the surface groups of Z-Fe (Eq. 7 and 9) are responsible for the lowest ammonium sorption at acidic pH values (near pH 2) due to competition with H^+ ions. The NH_4^+ sorption pH dependence exhibited an unexpected increase even above a pH of 9.3 when it is converted to NH_3, and then, the removal values could not be explained by the exchange reaction defined by Eq. 10 [39]. However, Liu et al. [20] reported Fe(III) removal of NH_3 due to a complexation reaction with Fe atoms as $\cong FeOH_n(NH_3)_m$.

$$Z\text{-}Na^+ + NH_4^+ \leftrightarrow Na^+ + Z\text{-}NH_4^+ \quad (10)$$

3.3. Effect of competing ions on phosphate and ammonium sorption

The phosphate sorption exhibited a slight improvement in the presence of Mg^{2+} (6 %) > K^{+} (5 %) > Na^{+} (3 %) and Ca^{2+} (1 %), which it has been reported for a synthetic zeolite due to the effect of a precipitation reaction involving the formation of $Mg/NH_4/PO_4$ and Ca/PO_4 minerals [40]. However, no mineralogical phase was identified by XRD analysis of the loaded iron samples due to their content being below the limit of detection. An important decrease in the ammonium removal was promoted by K^{+} (18 %) > Ca^{2+} (16 %) > Na^{+} (10 %) > Mg^{2+} (4 %), which is in agreement with the behaviour reported for a synthetic zeolite [5] even though the ion-exchange coefficients are favoured for NH_4^{+} ions over $K^{+}/Na^{+}/Ca^{2+}$ and Mg^{2+}. The cation mixture decreases by 16% and 38 % for the phosphate and ammonium uptakes, respectively.

The phosphate and ammonium sorption capacity has a variation of less 5 % in the presence of chloride and sulfate as reported for other zeolites (Figure 3) [5, 39]. Therefore, there is no competition between these species for the same binding sites due to outer-sphere complexation [40, 41]. Notably, a reduction in the phosphate removal was promoted by the coexistence of HCO_3^{-}, which is consistent with the selectivity reported for a modified zeolite [42]. The combination of anions decreases the phosphate and ammonium uptake by 8 % and 14 %, respectively.

The Langmuir isotherm ($R^2 \geq 0.99$) provided a better description of the phosphate and ammonium equilibrium sorption in the presence of competing ions compared with the Freundlich isotherm (Table 3, Figure 4). The ammonium sorption capacity decreased in the presence of ions at 23 mg-N/g and at 25mg-N/g with coexisting anions and cations. Similarly, decrease in the phosphate uptake capacity was observed in the presence of ions and anions at 3.1 mg-P/g and in the presence of cations at 3.3 mg-P/g.

3.4. Phosphate and ammonium sorption kinetics

The sorption kinetics of both the phosphate and ammonium ions for Z-Fe are comparable to those reported for zeolitic materials (Figure 5). Equilibrium was reached within 200 minutes, and

the phosphate sorption rates were lower compared with those of the ammonium ions, which is due to ion exchange between NH_4^+ and Na^+ ions being faster than phosphate ion complexation on the zeolite surface (≅FeOH).

The intraparticle diffusion model reported by Weber and Morris [43] (Eq. 11) was employed to describe the sorption mechanisms of the zeolite assuming it was promoted by diffusion in the spherical adsorbent and convective diffusion in the adsorbate solution.

$$q_t = k_t\, t^{1/2} + A \qquad (11)$$

where k_t ($mg.g^{-1}.h^{-1/2}$) is the intraparticle diffusion rate constant and A (mg/g) describes the thickness of the boundary layer (i.e., the higher the value of A, the greater the boundary layer effect). The sorption process is controlled by intraparticle diffusion when the sorption uptake (q_t) as a function of $t^{1/2}$ yields a straight line. In contrasts, when two or more steps influence the sorption process, the data result in multi-linear plots.

The fitting of the kinetic data to the intraparticle diffusion model revealed two linear steps. Therefore, film diffusion followed by particle diffusion may be used to describe the phosphate and ammonium sorption [44]. In addition, the phosphate and ammonium sorption were evaluated based on the film diffusion (D_f) and particle diffusion (D_p) mechanisms corresponding to the homogenous particle diffusion model (HPDM) (Figure 6) [45, 46]. The effective particle diffusivity calculates the sorption on the spherical particles using Eq. 12:

$$-\ln\left(1-\left(\frac{q_t}{q_e}\right)^2\right) = \frac{2\,\pi^2 D_p}{r^2}\,t \qquad (12)$$

When the rate of sorption is controlled by liquid film diffusion, this rate can be expressed as shown in Eq. 13:

$$-\ln\left(1-\left(\frac{q_t}{q_e}\right)\right) = \frac{D_f C_s}{h\,r\,C_z}\,t \qquad (13)$$

where q_t and q_e are the solute loadings on the adsorbent phase at time t and equilibrium (mg/g), respectively, C_s (mg/L) and C_z (mg/kg) are the ion concentrations in solution and in the zeolite, respectively, r is the average radius of the zeolite particles ($1x10^{-4}$ m), t is the contact time (min) and h is the thickness of film around the zeolite particle ($1x10^{-5}$ m for a poorly stirred solution) [47].

Both the phosphate and ammonium sorption exhibited higher values of D_f than those found for D_p. Therefore, particle diffusion was the rate-limiting step, and monolayer molecular sorption occurred on the surface of zeolite (Table 4), which is consistent with the results reported for ammonium sorption on natural zeolites at low initial ammonium concentrations [44, 47, 48]. In addition, the evaluation of the sorption kinetics was performed via convention models (supporting information Eqs. S1 – S2 and Table S1).

Based on FSEM – EDAX analysis, the loaded Z-Fe possessed a surface covered by several lamellar particles (supporting information Figure S3d), and the existence of phosphorus but not nitrogen was observed, which may be due to the content being below the limit of quantification. After sorption, the zeolite surface exhibited a compact crystalline framework. The loaded zeolite spectra (supporting information Figure S5) exhibited changes in the bands at 3392 cm^{-1}, 1455 cm^{-1} and 1040 cm^{-1} due to the hydroxyl groups (Fe(OH)) of the zeolite surface participating in the complexation reactions with the phosphate and ammonium ions [9, 49, 50]. Therefore, the increase in phosphate removal at the expense of a slight reduction in ammonium sorption occurred on Z-N and Z-Fe due to binding site competition.

3.5. Phosphorus speciation in the loaded Z-Fe samples

The L-B and R-P were the minor fractions of the immobilized phosphorous at 4±2 % and 3±2 %, respectively (Table 5), which is in agreement with previous results using a synthetic zeolite [51]. The 54±8 % phosphorus was associated with the iron and aluminum hydroxides. This result suggests that the Fe-OH groups of the hydrated iron oxides in Z-Fe are primarily responsible for phosphate removal. In addition, 39±6 % of phosphorus was immobilized by calcium and

magnesium (Ca+Mg)-P compounds. Chemical precipitation encouraged phosphate uptake but no mineral phase was determine by XRD analysis due to the concentrations being below the limit of quantification.

3.6. Phosphate and ammonium batch desorption

Higher recovery ratios were obtained for ammonium than phosphate from the loaded zeolite using NaOH, $NaHCO_3$, Na_2CO_3 and mixtures of $NaHCO_3$/Na_2CO_3 in the first sorption – desorption cycle (Table 6).

The partial phosphate desorption was due to complexation between hydrated iron oxide groups and phosphate and the formation of Ca-Mg phosphate mineral phases. All of the regenerated Z-Fe samples exhibited a larger decrease in phosphate uptake compared with ammonium removal capacity in the subsequent sorption cycles. Therefore, in operational terms, the sorption capacity obtained in the impregnation step was lost. Previous studies of Fe-loaded zeolites do not discuss general regeneration cycles and reuse, and loading capacity losses have not been previously reported. Therefore, the reuse of the modified zeolite will require re-impregnation after cycling, or the loaded zeolites could be potentially used for improvement of soil quality.

3.7. Simultaneous phosphate and ammonium uptake in dynamic assays

The breakthrough curves of ammonium (25 mg/L) and phosphate (12.5 mg/L) sorption by Z-Fe with and without competing ions are shown in Figure 7. The ammonium maximum sorption capacity at column saturation (C/C_0=0.95) was 26 mg-N/g at 306 BV, and in the presence of competing ions, the ammonium maximum sorption capacity decreased to 15 mg-N/g at 257 BV. In addition, the phosphate maximum sorption capacity decreased from 2.7 mg P/g at 167 BV to 1.1 mg-P/g at 122 BV in the presence of coexisting ions.

The profiles of the ammonium and phosphate desorption in a NaOH solution (Figure 8) indicated a recovery of 88±3 % of the eluted phosphate and 92±2 % of the eluted ammonium at 4 BV. The highest concentrations were determined to be 131 mg-P/L and 3834 mg-P/L. Under these

conditions, enrichment factors of 40 and 80 were achieved for phosphate and ammonium, respectively.

4. Conclusions

In this study, a simple modification process of an iron zeolite (Fe(III)) resulted in simultaneous cationic and anionic sorption. The enhancement of the phosphate uptake slightly affected the ammonium exchange capacity of the modified zeolite. The ammonium sorption primarily occurred by ion exchange and complexation with the (ZO^-) groups of the zeolitic structure and a combination of electrostatic interactions, chemical precipitation and inner sphere complexation with ≅Fe-OH functional groups act as the sorption mechanism for phosphate uptake. The coexistence of competing ions slightly affected the phosphate and ammonium sorption uptake onto Z-Fe. In the dynamic experiments, the desorption using 1 M NaOH provided enrichment factors of 39 and 80 for phosphate and ammonium, respectively. However, the sorption – desorption operation revealed a reduction in the anionic and cationic uptake capacity. Therefore, re-impregnation steps are required after reuse cycles, or based on the reusability limitations, the loaded zeolites have the potential for use as additives to improve soil quality.

Acknowledgments

This research was financially supported by Ministry of Science and Innovation through the ZERODISCHARGE project (CPQ2011-26799) and the Catalan government (project ref. 2009SGR905, 2014SGR050). The authors gratefully acknowledge R. Estany (Aigues de Barcelona), M. Gullom (EMMA), I. Sancho (Centro Tecnologíco del Agua (CETaqua)). Zeocem (Slovakia) for zeolites supply. Finally, I. Lopez (Laboratory of Electronic Microscopy, Universitat Politècnica de Catalunya) for the FSEM analysis and to N. Moreno (IDAEA-CSIC) for XRD determinations. Diana Guaya acknowledges the financial support of Secretaría de Educación Superior, Ciencia, Tecnología e Innovación (Senescyt - Ecuador) and Universidad Técnica Particular de Loja - Ecuador (Project - 2014: PROY_QUI_826).

References

1. Zamparas M, Drosos M, Georgiou Y, Deligiannakis Y and Zacharias I, A novel bentonite-humic acid composite material Bephos™ for removal of phosphate and ammonium from eutrophic waters. *Chem Eng J* **225**: 43-51 (2013).
2. Yin H and Kong M, Simultaneous removal of ammonium and phosphate from eutrophic waters using natural calcium-rich attapulgite-based versatile adsorbent. *Desalination* **351**: 128-137 (2014).
3. Villanueva ME, Salinas A, Copello GJ and Díaz LE, Point of zero charge as a factor to control biofilm formation of Pseudomonas aeruginosa in sol-gel derivatized aluminum alloy plates. *Surf Coat Technol* **254**: 145-150 (2014).
4. Król M, Mozgawa W, Jastrzębski W and Barczyk K, Application of IR spectra in the studies of zeolites from D4R and D6R structural groups. *Microporous Mesoporous Mater* **156**: 181-188 (2012).
5. Zhang M, Zhang H, Xu D, Han L, Niu D, Tian B, Zhang J, Zhang L and Wu W, Removal of ammonium from aqueous solutions using zeolite synthesized from fly ash by a fusion method. *Desalination* **271**: 111-121 (2011).
6. Alshameri A, Ibrahim A, Assabri AM, Lei X, Wang H and Yan C, The investigation into the ammonium removal performance of Yemeni natural zeolite: Modification, ion exchange mechanism, and thermodynamics. *Powder Technol* **258**: 20-31 (2014).
7. Malekian R, Abedi-Koupai J, Eslamian SS, Mousavi SF, Abbaspour KC and Afyuni M, Ion-exchange process for ammonium removal and release using natural Iranian zeolite. *Appl Clay Sci* **51**: 323-329 (2011).
8. Jiménez-Cedillo MJ, Olguín MT, Fall C and Colín A, Adsorption capacity of iron- or iron–manganese-modified zeolite-rich tuffs for As(III) and As(V) water pollutants. *Appl Clay Sci* **54**: 206-216 (2011).

9. Huang H, Xiao D, Pang R, Han C and Ding L, Simultaneous removal of nutrients from simulated swine wastewater by adsorption of modified zeolite combined with struvite crystallization. *Chem Eng J* **256**: 431-438 (2014).

10. Haque N, Morrison G, Cano-Aguilera I and Gardea-Torresdey JL, Iron-modified light expanded clay aggregates for the removal of arsenic(V) from groundwater. *Microchemical Journal* **88**: 7-13 (2008).

11. Villalba JC, Constantino VRL and Anaissi FJ, Iron oxyhydroxide nanostructured in montmorillonite clays: Preparation and characterization. *J Colloid Interface Sci* **349**: 49-55 (2010).

12. Iesan CM, Capat C, Ruta F and Udrea I, Evaluation of a novel hybrid inorganic/organic polymer type material in the Arsenic removal process from drinking water. *Water Res* **42**: 4327-4333 (2008).

13. Cumbal L, Greenleaf J, Leun D and SenGupta AK, Polymer supported inorganic nanoparticles: characterization and environmental applications. *React Funct Polym* **54**: 167-180 (2003).

14. Jeon C-S, Baek K, Park J-K, Oh Y-K and Lee S-D, Adsorption characteristics of As(V) on iron-coated zeolite. *J Hazard Mater* **163**: 804-808 (2009).

15. Li Z, Jiang W-T, Jean J-S, Hong H, Liao L and Lv G, Combination of hydrous iron oxide precipitation with zeolite filtration to remove arsenic from contaminated water. *Desalination* **280**: 203-207 (2011).

16. Bilici Baskan M and Pala A, Removal of arsenic from drinking water using modified natural zeolite. *Desalination* **281**: 396-403 (2011).

17. Li Z, Jean J-S, Jiang W-T, Chang P-H, Chen C-J and Liao L, Removal of arsenic from water using Fe-exchanged natural zeolite. *J Hazard Mater* **187**: 318-323 (2011).

18. Šiljeg M, Stefanović ŠC, Mazaj M, Tušar NN, Arčon I, Kovač J, Margeta K, Kaučič V and Logar NZ, Structure investigation of As(III)- and As(V)-species bound to Fe-modified clinoptilolite tuffs. *Microporous Mesoporous Mater* **118**: 408-415 (2009).

19. Dávila-Jiménez MM, Elizalde-González MP, Mattusch J, Morgenstern P, Pérez-Cruz MA, Reyes-Ortega Y, Wennrich R and Yee-Madeira H, In situ and ex situ study of the enhanced modification with iron of clinoptilolite-rich zeolitic tuff for arsenic sorption from aqueous solutions. *J Colloid Interface Sci* **322**: 527-536 (2008).

20. Liu H, Yang L, Ma M, Li P and Wei Y, The transformation of ferrihydrite in the presence of trace Fe(II): The effect of the ammonia, amine and the coordination ions of Fe(III). *Journal of Solid State Chemistry* **183**: 542-546 (2010).

21. Jiménez-Cedillo MJ, Olguín MT and Fall C, Adsorption kinetic of arsenates as water pollutant on iron, manganese and iron–manganese-modified clinoptilolite-rich tuffs. *J Hazard Mater* **163**: 939-945 (2009).

22. Kim KS, Park JO and Nam SC, Synthesis of Iron-loaded Zeolites for Removal of Ammonium and Phosphate from Aqueous Solutions. *Environ Eng Res* **18**: 267-276 (2013).

23. Hieltjes AHM and Lijklema L, Fractionation of Inorganic Phosphates in Calcareous Sediments1. *J Environ Qual* **9**: 405-407 (1980).

24. APHA A, WEF., Standard methods for the examination of water and wastewater. American Public Health Association, American Water Works Association, and Water Environment Federation (2000).

25. Lei L, Li X and Zhang X, Ammonium removal from aqueous solutions using microwave-treated natural Chinese zeolite. *Sep Purif Technol* **58**: 359-366 (2008).

26. Doula MK, Synthesis of a clinoptilolite–Fe system with high Cu sorption capacity. *Chemosphere* **67**: 731-740 (2007).

27. Margeta K, Logar NZ, Šiljeg M and Farkaš A, Natural Zeolites in Water Treatment – How Effective is Their Use, in Water Treatment, ed by Elshorbagy W and Chowdhury RK. InTech, Rijeka, pp. 81-112 (2013).

28. Reháková M, Fortunová Ľ, Bastl Z, Nagyová S, Dolinská S, Jorík V and Jóna E, Removal of pyridine from liquid and gas phase by copper forms of natural and synthetic zeolites. *J Hazard Mater* **186**: 699-706 (2011).

29. Li J, Qiu J, Sun Y and Long Y, Studies on natural STI zeolite: modification, structure, adsorption and catalysis. *Microporous Mesoporous Mater* **37**: 365-378 (2000).

30. Luan Z and Fournier JA, In situ FTIR spectroscopic investigation of active sites and adsorbate interactions in mesoporous aluminosilicate SBA-15 molecular sieves. *Microporous Mesoporous Mater* **79**: 235-240 (2005).

31. Jin F and Li Y, A FTIR and TPD examination of the distributive properties of acid sites on ZSM-5 zeolite with pyridine as a probe molecule. *Catal Today* **145**: 101-107 (2009).

32. Lǔ J, Liu H, Liu R, Zhao X, Sun L and Qu J, Adsorptive removal of phosphate by a nanostructured Fe–Al–Mn trimetal oxide adsorbent. *Powder Technol* **233**: 146-154 (2013).

33. Dzombak D and Morel F, Surface Complexation Modeling: Hydrous Ferric Oxide. John Wiley & Sons, Inc., New York (1990).

34. Simsek EB, Özdemir E and Beker U, Zeolite supported mono- and bimetallic oxides: Promising adsorbents for removal of As(V) in aqueous solutions. *Chem Eng J* **220**: 402-411 (2013).

35. Sujana MG, Soma G, Vasumathi N and Anand S, Studies on fluoride adsorption capacities of amorphous Fe/Al mixed hydroxides from aqueous solutions. *J Fluorine Chem* **130**: 749-754 (2009).

36. Chitrakar R, Tezuka S, Sonoda A, Sakane K, Ooi K and Hirotsu T, Phosphate adsorption on synthetic goethite and akaganeite. *J Colloid Interface Sci* **298**: 602-608 (2006).

37. You X, Guaya D, Farran A, Valderrama C and Cortina JL, Phosphate removal from aqueous solution using a hybrid impregnated polymeric sorbent containing hydrated ferric oxide (HFO). *J Chem Technol Biotechnol*: n/a-n/a (2015).

38. Blaney LM, Cinar S and SenGupta AK, Hybrid anion exchanger for trace phosphate removal from water and wastewater. *Water Res* **41**: 1603-1613 (2007).

39. Huang H, Xiao X, Yan B and Yang L, Ammonium removal from aqueous solutions by using natural Chinese (Chende) zeolite as adsorbent. *J Hazard Mater* **175**: 247-252 (2010).

40. Guan Q, Hu X, Wu D, Shang X, Ye C and Kong H, Phosphate removal in marine electrolytes by zeolite synthesized from coal fly ash. *Fuel* **88**: 1643-1649 (2009).

41. Onyango MS, Kuchar D, Kubota M and Matsuda H, Adsorptive Removal of Phosphate Ions from Aqueous Solution Using Synthetic Zeolite. *Ind Eng Chem Res* **46**: 894-900 (2007).

42. Ning P, Bart H-J, Li B, Lu X and Zhang Y, Phosphate removal from wastewater by model-La(III) zeolite adsorbents. *J Environ Sci* **20**: 670-674 (2008).

43. Weber WJ and Morris JC, Kinetics of adsorption on carbon solution. *J San Eng Div* **89**: 31-59 (1963).

44. Lin L, Lei Z, Wang L, Liu X, Zhang Y, Wan C, Lee D-J and Tay JH, Adsorption mechanisms of high-levels of ammonium onto natural and NaCl-modified zeolites. *Sep Purif Technol* **103**: 15-20 (2013).

45. Helfferich FG, Ion exchange. McGraw-Hill, New York (1962).

46. Valderrama C, Barios JI, Caetano M, Farran A and Cortina JL, Kinetic evaluation of phenol/aniline mixtures adsorption from aqueous solutions onto activated carbon and hypercrosslinked polymeric resin (MN200). *React Funct Polym* **70**: 142-150 (2010).

47. Moussavi G, Talebi S, Farrokhi M and Sabouti RM, The investigation of mechanism, kinetic and isotherm of ammonia and humic acid co-adsorption onto natural zeolite. *Chem Eng J* **171**: 1159-1169 (2011).

48. Sprynskyy M, Lebedynets M, Zbytniewski R, Namieśnik J and Buszewski B, Ammonium removal from aqueous solution by natural zeolite, Transcarpathian mordenite, kinetics, equilibrium and column tests. *Sep Purif Technol* **46**: 155-160 (2005).

49. Guo J, Yang C and Zeng G, Treatment of swine wastewater using chemically modified zeolite and bioflocculant from activated sludge. *Bioresour Technol* **143**: 289-297 (2013).

50. Wahab MA, Boubakri H, Jellali S and Jedidi N, Characterization of ammonium retention processes onto Cactus leaves fibers using FTIR, EDX and SEM analysis. *J Hazard Mater* **241–242**: 101-109 (2012).

51. Xie J, Wang Z, Wu D and Kong H, Synthesis and properties of zeolite/hydrated iron oxide composite from coal fly ash as efficient adsorbent to simultaneously retain cationic and anionic pollutants from water. *Fuel* **116**: 71-76 (2014).

Element	Z-N	Z-Na	Z-Fe
O	57.8 ± 2.6	60.3 ± 1.4	57.4 ± 3.4
Na	0.3 ± 0.0	1.5 ± 0.1	0.4 ± 0.8
Mg	0.4 ± 0.1	0.4 ± 0.0	- ± -
Al	5.3 ± 0.2	5.3 ± 0.0	3.3 ± 1.4
Si	29.7 ± 1.7	29.1 ± 1.5	23.3 ± 3.7
Cl	< loq*	< loq*	1.1 0.2
K	2.9 ± 0.5	1.8 ± 0,2	1.0 ± 0.2
Ca	1.9 ± 0.3	1.1 ± 0,1	0.6 ± 1.0
Ti	0.2 0.2	< loq*	< loq*
Fe	1.6 ± 0.4	0.5 ± 0,0	12.8 ± 2.4

*loq: limit of quantification

Table 1. Chemical composition (wt. %) of the zeolitic materials: natural zeolite (Z-N), sodium zeolite (Z-Na) and iron zeolite (Z-Fe).

		Langmuir			Freundlich		
		q_m (mg/g)	K_L (L/mg)	R^2	K_F ((mg/g)/(mg/L)$^{1/n}$)	1/n	R^2
Z-N	Phosphate	0.6	0.01	0.99	0.02	0.47	0.97
	Ammonium	33	0.006	0.99	1.84	0.36	0.94
Z-Fe	Phosphate	3.4	0.02	0.99	0.59	0.25	0.71
	Ammonium	27	0.004	0.99	0.80	0.46	0.96

Table 2. Isotherm parameters for phosphate and ammonium sorption on natural zeolite (Z-N) and iron zeolite (Z-Fe).

Langmuir	Freundlich

	q_m (mg/g)	K_L (L/mg)	R^2	K_F ((mg/g)/(mg/L)$^{1/n}$)	1/n	R^2
Phosphate	3.4	0.02	0.99	0.59	0.25	0.71
P-Anions	3.1	0.01	0.99	0.35	0.31	0.81
P-Cations	3.3	0.02	0.99	0.54	0.26	0.80
P-Ions	3.1	0.02	0.99	0.53	0.24	0.98
Ammonium	27	0.004	0.99	0.80	0.46	0.96
N-Anions	25	0.003	0.99	0.69	0.45	0.97
N-Cations	25	0.002	0.98	0.45	0.49	0.99
N-Ions	23	0.002	0.99	0.46	0.47	0.99

Table 3. Isotherm parameters for phosphate and ammonium sorption by iron zeolite (Z-Fe) in the presence of competing ions.

Model	Kinetic parameters	Phosphate	Ammonium
Intraparticle diffusion	k_{t1} (mg·g^{-1}·h$^{-1/2}$)	0.1	1.9
	R^2	0.99	0.97
	k_{t2} (mg·g^{-1}·h$^{-1/2}$)	0.1	0.5
	R^2	0.89	0.96
Film diffusion	D_f (m^2·s^{-1})	4.6x10^{-11}	1.2x10^{-09}
	R^2	0.92	0.95
Particle diffusion	D_p (m^2·s^{-1})	1.6x10^{-13}	2.1x10^{-12}
	R^2	0.98	0.98

Table 4. Kinetic parameters for phosphate and ammonium removal by iron zeolite (Z-Fe).

q_e	LB-P		(Fe+Al)-P		(Ca+Mg)-P (mg/g)		R-P	
(mg/g)	(mg/g)	%	(mg/g)	%	(mg/g)	%	(mg/g)	%

0.98	0.03	4±2	0.53	54±8	0.39	39±6	0.03	3±2

Table 5. Speciation of phosphate immobilized on the iron zeolite (Z-Fe) associated to the chemical forms: LB-P; (Fe+Al)-P; (Ca+Mg)-P; R-P.

Elution solution	Desorption (%)	
	Phosphate	Ammonium
1 M NaOH	64±4	92±6
0.1 M $NaHCO_3$	49±4	52±4
0.1 M Na_2CO_3	74±5	91±6
0.1 $NaHCO_3$/0.1 MNa_2CO_3	73±5	66±4

Table 6. Simultaneous phosphate and ammonium desorption efficiency from loaded Z-Fe in batch experiments at 21±ºC.

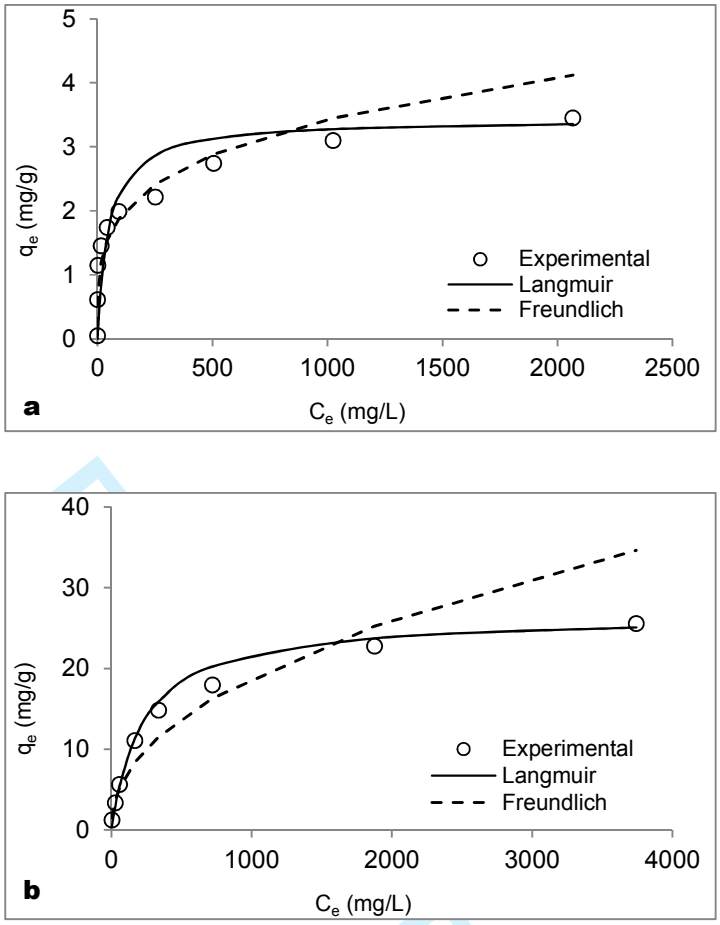

Figure 1. Experimental and theoretical equilibrium isotherms for a) phosphate and b) ammonium removal by iron zeolite (Z-Fe) at constant equilibrium pH 3.1±0.2.

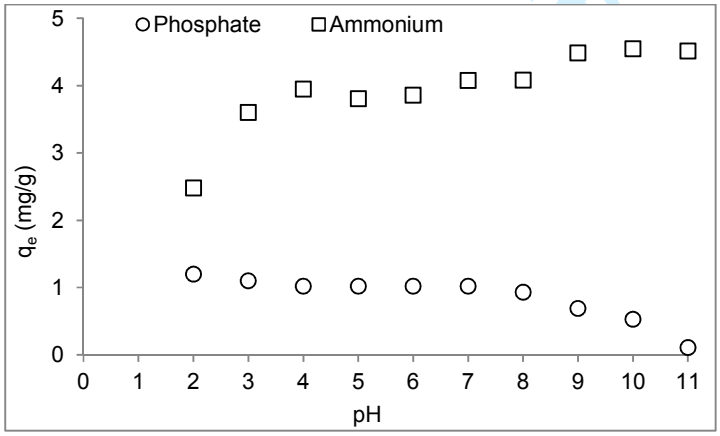

Figure 2. Effect of pH on the phosphate and ammonium removal by iron zeolite (Z-Fe).

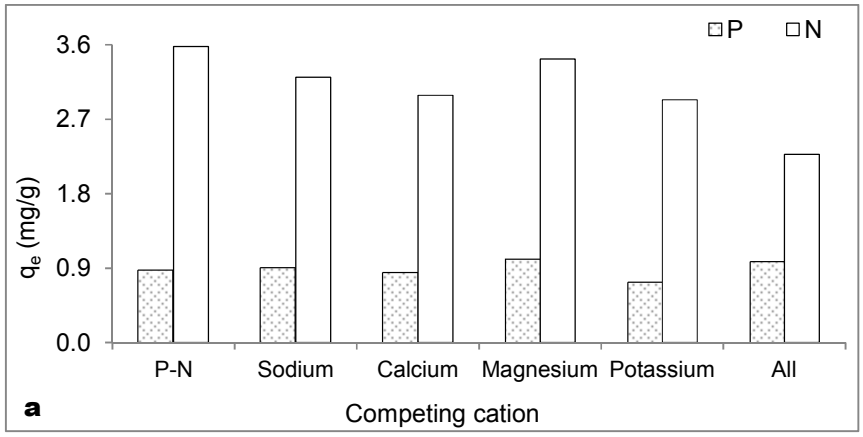

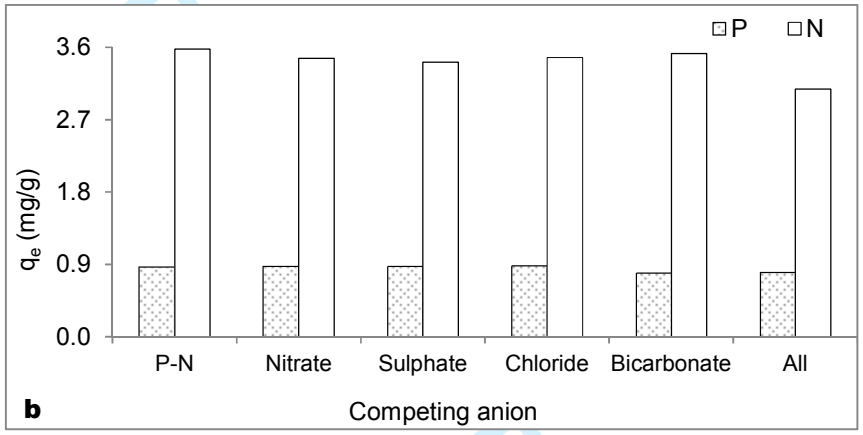

Figure 3. Individually effect of a) cations and b) anions for phosphate (P) and ammonium (N) removal by iron zeolite (Z-Fe).

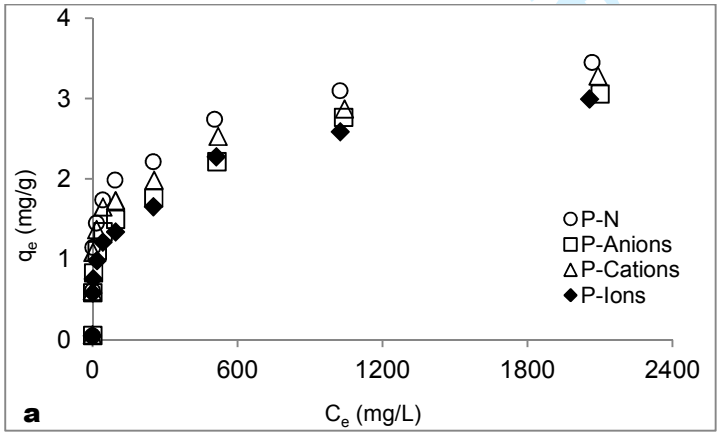

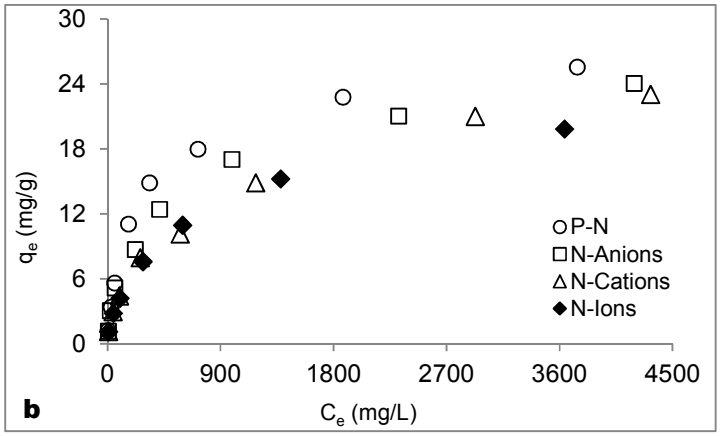

Figure 4. Equilibrium capacity for a) phosphate and b) ammonium recovery by the iron zeolite (Z-Fe) in presence of competing ions.

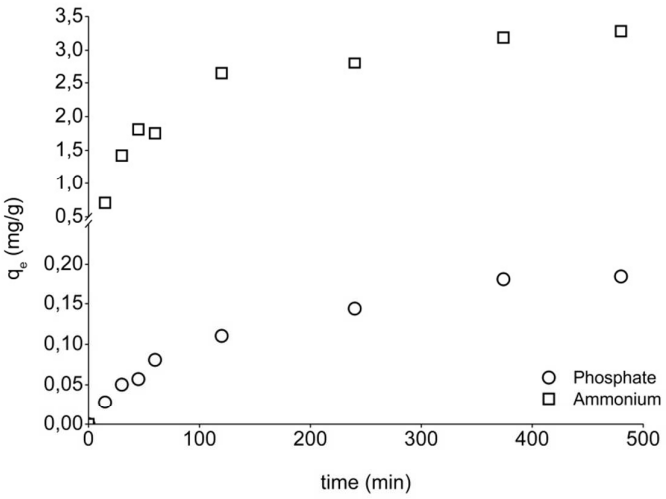

Figure 5. Evolution of phosphate and ammonium sorption uptake versus time for iron zeolite (Z-Fe) in batch experiments at 21±1 ºC.

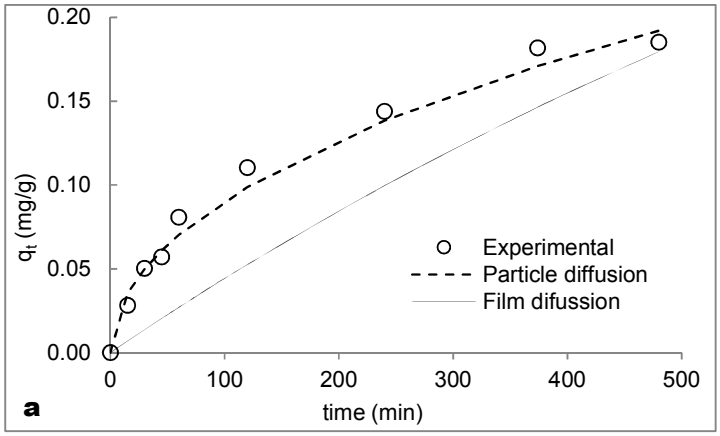

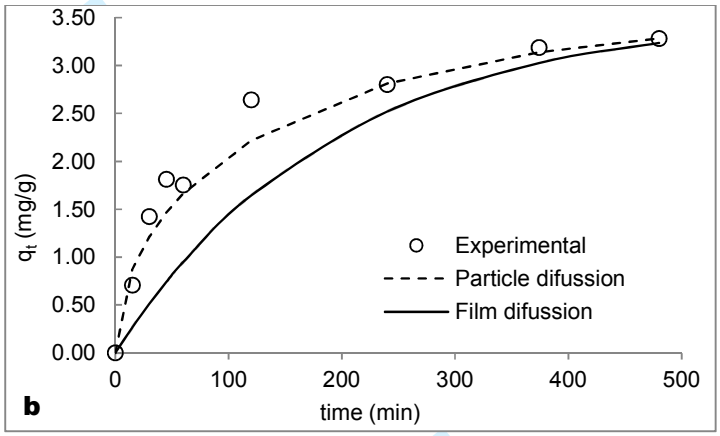

Figure 6. Experimental and theoretical sorption kinetics of a) phosphate and b) ammonium ions for Z-Fe.

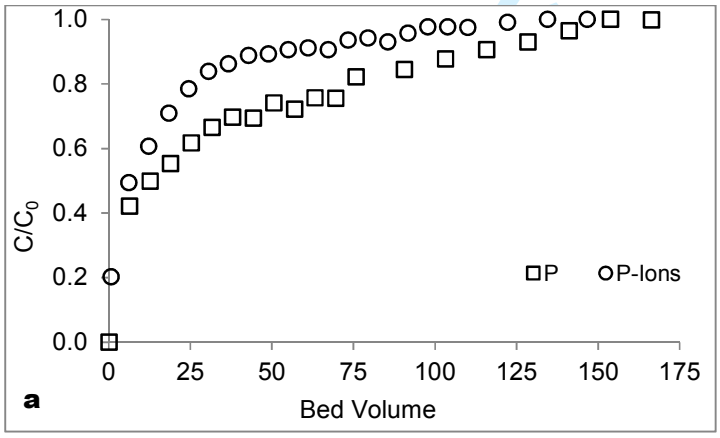

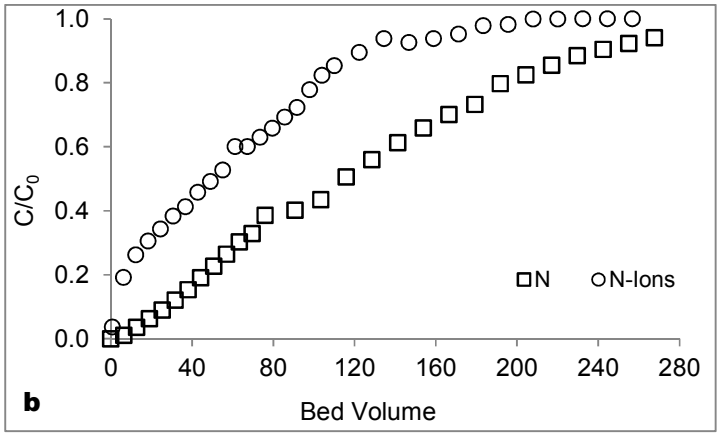

Figure 7. Breakthrough curves of a) phosphate and b) ammonium uptake by iron zeolite (Z-Fe) at flow rate of 1.8 mL/min.

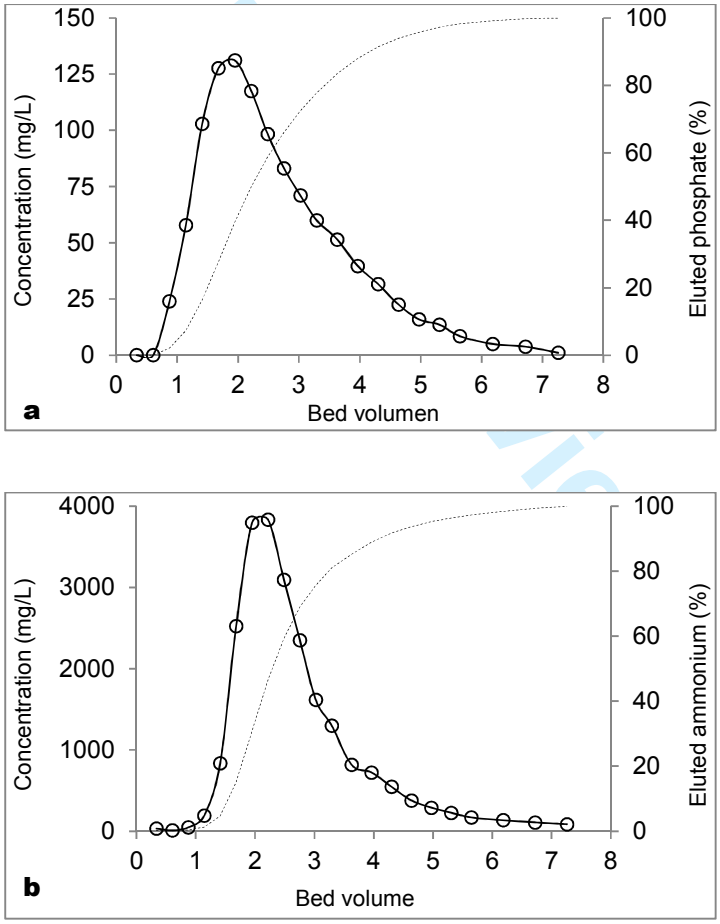

Figure 8. Desorption profiles of a) phosphate and b) ammonium from loaded iron zeolite (Z-Fe) using 1 M NaOH at 0.5 mL/min.